Available online at www.sciencedirect.com

SciVerse ScienceDirect

Ceramics International 39 (2013) 93–99

CERAMICS INTERNATIONAL

www.elsevier.com/locate/ceramint

Investigation of shrinkage control in Ni–Al_2O_3 (Metal–Ceramic) functionally graded materials

Seungkyu Yang, Hyungsub Kim, Caroline Sunyong Lee*

Department of Materials Engineering, Hanyang University, Ansan-si, Kyunggi-do 426-791, Republic of Korea

Received 20 March 2012; received in revised form 16 May 2012; accepted 27 May 2012
Available online 13 June 2012

Abstract

Nickel–alumina (metal–ceramic) graded composites were fabricated based on empirical relationships that were used to predict shrinkage expected during the sintering process. Compositions ranged from pure Al_2O_3 to nickel. Compositions with different sintering behaviors were composed of Ni powders having 3-μm particles and Al_2O_3 powders having 0.16-μm particles that were mixed in specific volume percentages. The green and sintered densities were measured for each layer of the multi-layered samples. Based on these measurements, an empirical formulation for shrinkage was derived to express the relationship between green and sintered densities. Shrinkage was predicted from the observed decrease in porosity during sintering. This was used to establish a relationship between shrinkage and composition. Dramatic shrinkage, which can lead to cracking of the sample, was resolved by minimizing shrinkage differences within the functionally graded materials using the derived empirical formulation for shrinkage; internal cracking was significantly reduced by maintaining a consistent shrinkage gradient.

Keywords: Functionally graded material (FGM); Pressureless sintering; Compacts/compaction; Al_2O_3 matrix composites

1. Introduction

Functionally graded material (FGM) bonding is a joining method that creates a continuous change in composition from one side of the bond to the other, with an accompanying gradient in thermal expansion properties. Numerous studies have described metal–ceramic FGMs that combine the high temperature resistance of ceramics with the toughness of metals [1–3]. There are several processing methods for fabricating FGMs. Powder metallurgy is a relatively simple, widely-used technique that allows one to accurately control composition [4–8,12,17]. However, the interior of FGMs can distort and bend because of non-uniform shrinkage during sintering, resulting in cracks [4,5].

An FGM fabricated using the powder compaction method may have non-uniform density gradients in the green body due to compositional differences within each layer, which can produce non-uniform shrinkage during sintering. This type of sintering stress has been observed in numerous studies of bilayer systems [9,10]. The problem becomes more serious in multi-layered samples because a single distortion or defect can affect other layers. Therefore, sintering stress and subsequent distortions are difficult to predict and control in multi-layer systems.

In this study, a multi-layered FGM model having uniform shrinkage is proposed to overcome problems associated with non-uniform distortion due to uneven green body density caused by varying composition of the various layers. Fig. 1 shows how a uniform shrinkage gradient can provide a crack-free FGM. While it is possible to measure shrinkage within each layer of an FGM, it is difficult to use these measured values to estimate shrinkage of the entire FGM. In general, shrinkage during sintering occurs through the removal of pores in a green body as sintering progresses. The degree of shrinkage can be predicted by changes in pore density as the materials are being sintered. Green and sintered densities have been studied extensively in order to identify material compositions having predictable shrinkage.

*Correspondence to: Department of Materials Engineering, Hanyang University, Room #312, 5th Engineering Building, 55 hanyangdaehak-ro, Sangnok-gu, Ansan-si, Gyeonggi-do 426-791, Republic of Korea.
Tel.: +82 31 400 5221; fax: +82 31 436 8146.
E-mail address: sunyonglee@hanyang.ac.kr (C. Sunyong Lee).

0272-8842/$36.00
http://dx.doi.org/10.1016/j.ceramint.2012.05.100

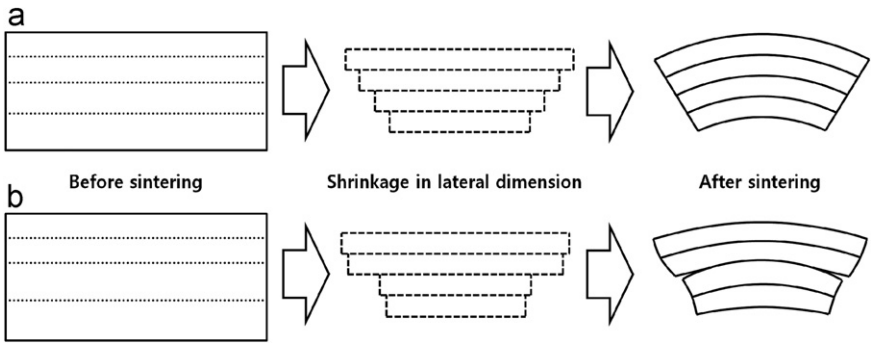

Fig. 1. Schematic diagram of FGMs with (a) uniform and (b) non-uniform shrinkage gradients.

Here, a mathematical expression based on the measured green and sintered densities of each layer of an FGM was derived to predict the shrinkage of a material based on its component distribution. The expression was applied to a multi-layered system to fabricate an FGM having a uniform shrinkage distribution. To obtain a crack-free FGM, crack propagation was minimized by designing a uniform shrinkage gradient based on measured non-uniform shrinkages of the individual layers in FGM samples during sintering.

2. Experimental procedure

2.1. Sample fabrication

FGMs were prepared from powder mixtures with various volume fractions of Ni and Al_2O_3. The powders had average particle sizes of 3 μm for Ni (Sigma-Aldrich, USA) and 0.16 μm for Al_2O_3 (Taimicron, Japan). These powders were used in all the layers. To ensure homogeneous mixing of the powders, the powder mixtures were dispersed in ethanol, the suspension was ultrasonicated, and the ethanol evaporated to dryness. The dried powders were passed through a 100-mesh sieve to ensure a uniform powder size fraction.

Mixed powders for each layer were cold-pressed (CP) uniaxially in a round WC die (12 mm in diameter) at a pressure of 133 MPa. Cold isostatic pressing (CIP) at a pressure of 150 MPa was then used to homogeneously compact the green bodies. Archimedes' method was used to measure green densities after pressing. The green bodies were sintered in a tube furnace in an Ar atmosphere at 1 atm to prevent Ni oxidation. The maximum sintering temperature, 1350 °C, was maintained for 3 h. The heating rate was 4 °C/min, and the cooling rate was 2 °C/min. After sintering, the density of the sintered body for each sample was measured using the Archimedes method (Tables 1 and 2).

A dilatometer was used to monitor shrinkage at different temperatures in order to relate shrinkage to density. Five selected compositions (0, 10, 50, 90, and 100 vol% nickel) were measured.

2.2. FGM fabrication

Relationships between composition and sintered density, and between composition and green density, were developed using the densities of each FGM composition. A mathematical expression based on these relationships was used to calculate shrinkage distributions based on composition. The theoretical results were compared with those obtained with the dilatometer. Using these data, an FGM was fabricated with a composition that had a uniform shrinkage distribution.

An FGM sample was CP in a WC die (1-inch diameter) at 133 MPa, followed by CIP at 150 MPa. The powders used and the sintering conditions were as stated above. Three FGMs with different layer compositions were fabricated, as listed in Table 1. Sample A, whose composition changed axially across the layers, was fabricated to compare with the samples created in accordance with the derived mathematical

Table 1
Compositions of the fabricated FGMs.

Layer	Sample A	Sample B (vol% Ni)	Sample C
1	0	0	0
2	10	5	11.5
3	20	10	22
4	30	20	32
5	40	30	41.5
6	50	40	50
7	60	60	60
8	70	70	80
9	80	85	100
10	90	100	–
11	100	–	–

Table 2
Optimized composition of each layer in Sample C with a uniform shrinkage gradient.

Layer	Expected shrinkage	Volume fraction of Ni	Theoretical density (g/cm^3)
1	0.178	0.000	3.98
2	0.164	0.115	4.55
3	0.150	0.220	5.06
4	0.136	0.320	5.56
5	0.122	0.415	6.03
6	0.108	0.500	6.45
7	0.094	0.600	6.94
8	0.081	0.800	7.92
9	–	1.000	8.91

expression. The composition of Sample B (Park et al. [12]) was designed to minimize thermal expansion mismatch during cooling. Sample A was also compared to the fabricated Sample C, whose composition was designed using the empirical shrinkage model that was developed in this study. Scanning electron microscopy (SEM) and optical microscopy (OM) were used to study the microstructure and shrinkage within the FGM.

3. Results and discussion

3.1. Sintering behavior

Fig. 2 shows the shrinkage of five different compositions measured with the dilatometer for samples heated from room temperature to 1350 °C. As shown in the figure, sintering of the 100 vol% Ni sample began around 585 °C, whereas sintering of the 100 vol% Al_2O_3 sample started around 965 °C. The other compositions were sintered at intermediate temperatures. The dilatometer results indicated that the distortion caused by different degrees of shrinkage among the layers was not only due to the final shrinkage amount but also due to differences between the onset sintering temperatures. Fig. 2 shows that 100% Ni and 100% Al_2O_3 samples had different onset sintering temperatures. This difference in onset sintering temperatures between Ni and Al_2O_3 can cause distortion in the sample, which can lead to cracking in the sample. Therefore, maintaining a uniform sintering behavior was just as important as the final amount of shrinkage [7]. To achieve the former, the composition of the Al_2O_3 matrix was held constant across the layers by using powders of fixed particle sizes, i.e., 0.16 μm for Al_2O_3 and 3 μm for Ni. As a result, consistent shrinkage differences occurred throughout the layers with the exception of the 100 vol% Ni composition.

3.2. Prediction of shrinkage

Fig. 3 shows the density distribution of each composition across the FGM; the density for each composition was measured by Archimedes' method. As shown in the figure, powder mixtures with bimodal distributions improved the green density because small particles fill the pores between larger particles [11]. The highest green density was measured for the 58 vol% Ni composition (Fig. 3). In order to empirically express the sintered density, two factors were considered: first, green density influenced the final sintered density. Therefore, different factors, α and β, were used in the empirical calculation of final sintered density to consider its two separate regions of green body density as shown in Fig. 3. Second, the sintered density of the

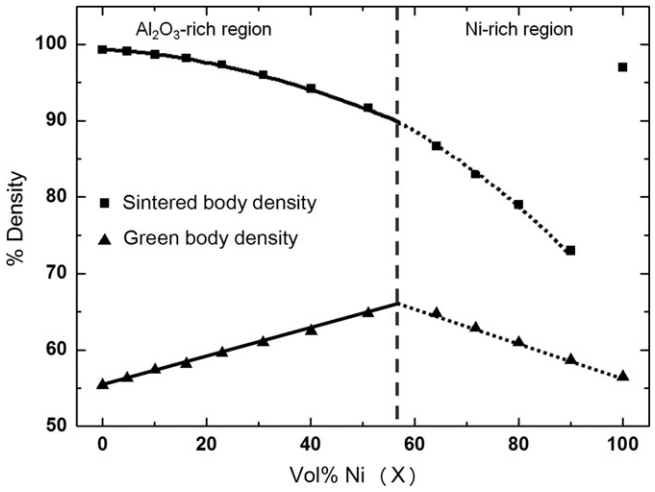

Fig. 3. Distribution of green and sintered densities for each composition. The lines above the green body density are the calculated sintered densities using Eq. (1). The square markers represent experimentally-measured sintered densities.

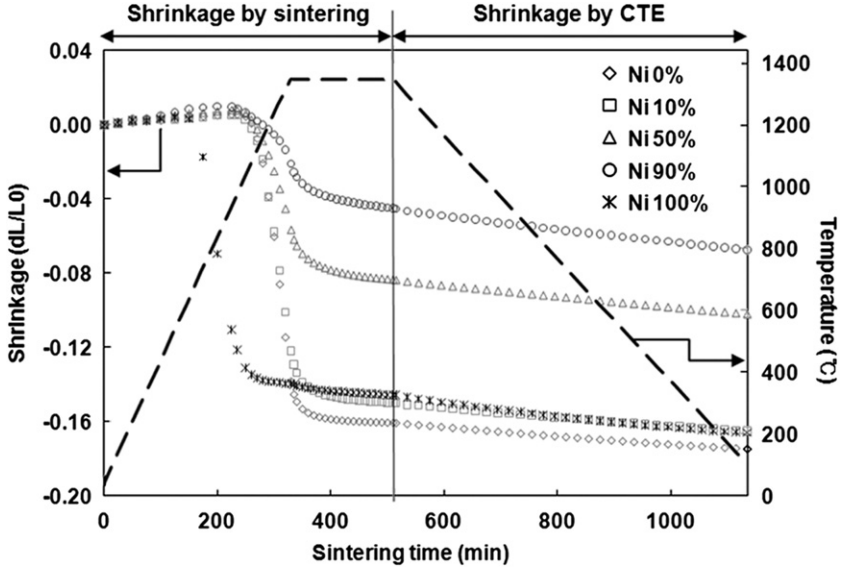

Fig. 2. Shrinkage measured by a dilatometer for samples sintered according to the heating profile indicated by the dashed line.

Al_2O_3 matrix composite decreased as the amount of Ni increased. Sintered density can be expressed empirically as

$$\rho = \rho' - \beta X^{\alpha} \quad (1)$$

where ρ is the calculated final sintered density and ρ' is the experimentally-measured sintered density of 100% (pure) Al_2O_3. Pure Al_2O_3 was taken as a reference because the matrix in this FGM was Al_2O_3. X is the volume fraction of the nickel powder added to the matrix, α is an exponential factor expressing the decrease in sintered density based on the added powders, and β is a constant for fitting the equation. We assumed that the sintered density decreased as Ni content increased, as verified by experimentally-measured values (Fig. 3). The Ni content and the green density both influenced sintered density. As the green density increased, the relative sintered density increased, and *vice versa*. As shown in Fig. 3, green density increased to a maximum at 58 vol% Ni, then decreased steadily. Therefore, green density distribution was divided into two regions based on 58 vol% Ni where different factors such as α and β, were used in the equation depending on the nickel content. The factors used in the Al_2O_3-rich region were 1.7 for α and 0.0095 for β. The factors used in the Ni-rich region were 2.3 for α and 0.00084 for β. These constants were experimentally derived.

Generally, for bimodal distributions of the same type of powder, sintered density decreases with increasing particle size because powders composed of large particles do not have large specific surface areas for extensive necking [11]. However, the current study is based on the sintering of two different kinds of powders, where the maximum density was observed only when those two components were sintered separately. Moreover, as the proportion of Al_2O_3 powder in the matrix decreased, sintered density also decreased. This is similar to the behavior of bimodal distributions previously observed with the same type of powders. In order to apply Eq. (1) to the shrinkage model, one must assume that the matrix (alumina in this case) is distributed uniformly throughout the sample. Sintering behavior can then be predicted based on this assumption. In addition, it is possible to relate changes in porosity to shrinkage using Eq. (2) derived by Bruck et al. [6,17]:

$$\varepsilon = 1 - \left(\frac{1-P_i}{1-P_f}\right)^{1/3} \quad (2)$$

where P_i is the porosity of the green body, P_f is the porosity of the sintered body and ε is the 1-dimensional shrinkage at a specific composition. This equation assumes isotropic shrinkage.

Fig. 4 uses Eq. (2) to compare measured and predicted shrinkages at various volume fractions of Ni; $1-P_i$ in Eq. (2) is a measured green density for each volume fraction which is shown in Figs. 3 and $1-P_f$ in this equation is ρ for each composition in Eq. (1) which is the points plotted for sintered body density. Based on these values, Fig. 4 plots calculated shrinkage (ε) from Eq. (2) and measured shrinkage using dilatometer. Again, shrinkage

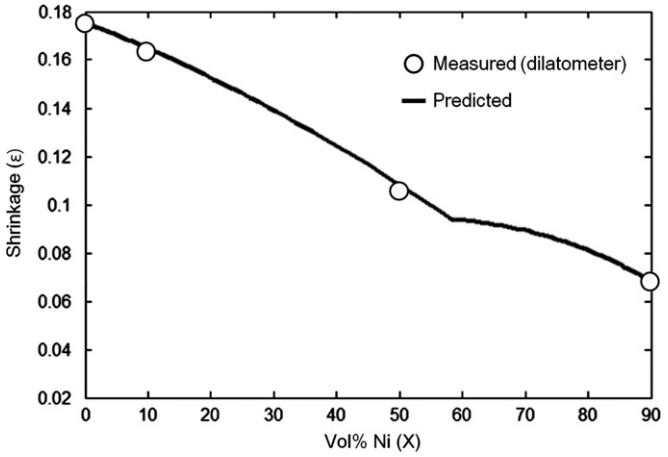

Fig. 4. Measured and calculated shrinkages at various volume fractions of Ni.

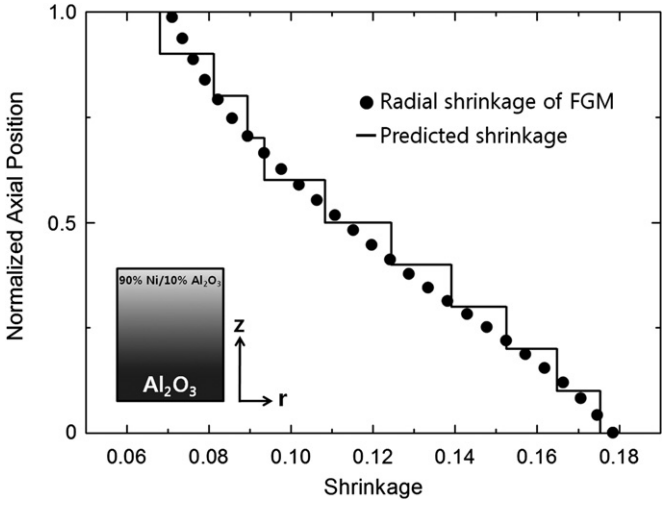

Fig. 5. Comparison of measured and predicted radial shrinkages of an FGM. The inset shows the location of the radial shrinkage measurement within the FGM.

was calculated in two different regions, as dramatic slope change in green density was observed at 58 vol% Ni composition. As shown in the figure, there is almost no difference between shrinkages measured by the dilatometer (Fig. 2) and the predicted values. Fig. 5 compares predicted with measured shrinkages of an FGM during sintering. The predicted shrinkage shown in Fig. 5 is based on Eq. (2), which was developed using this FGM. Fig. 5 compares the predicted shrinkage, which was experimentally derived, with the measured shrinkage of the fabricated FGM. The predicted shrinkage is shown as a step-function because the FGM is stacked layer-by-layer. The measured and predicted shrinkages agree, indicating that the derived empirical equations fit the experimental results.

In general, cracks in a multi-layered sample can occur in two ways. First, thermal expansion mismatch among layers can result in large residual stresses between layers, leading to cracking in the sample during cooling. Usually,

this problem can be resolved by stress analysis using a finite element method (FEM) study followed by adjusting the thickness of each layer to accommodate the stresses. Second, as a sample gets heated from room temperature to the high sintering temperature, differential shrinkage between different compositions can cause distortion within each layer, resulting in cracks.

Fig. 6 shows a cross-section of a fabricated FGM in which the thermal expansion mismatch was minimized. The distortion or bending observed in the fabricated FGM was as low as 2% of its diameter. Nonetheless, fine cracks were observed for the composition of 30 vol% Ni/70 vol% Al_2O_3. The FGM in Fig. 6 was graded, i.e., prepared with layers of steadily increasing Ni content, to obtain a smooth thermal expansion transition. However, the crack in this figure clearly shows that grading for a smooth thermal expansion transition is alone insufficient to provide an FGM free of cracks. Therefore, shrinkage caused by differences in the sintering onset temperatures plays an important role in obtaining crack-free FGMs.

3.3. Fabrication of an FGM having a uniform shrinkage gradient

Table 2 shows the layer compositions that provide a uniform shrinkage gradient. An FGM was fabricated based on these compositions (Figs. 7, 8 and 9). The values in Table 2 were obtained as follows: Eq. (2) was used to calculate the actual shrinkage for layer #1 (100% Al_2O_3, 0.178 shrinkage) and layer #8 (80 vol% Ni/20 vol% Al_2O_3, 0.081 shrinkage). These limits were then subdivided, and the shrinkages were estimated by linear interpolation for eight compositions spanning these extremes, as shown in the first column of Table 2. Fig. 4 was used to identify the corresponding composition for each shrinkage value; these compositions are shown in the second column of Table 2.

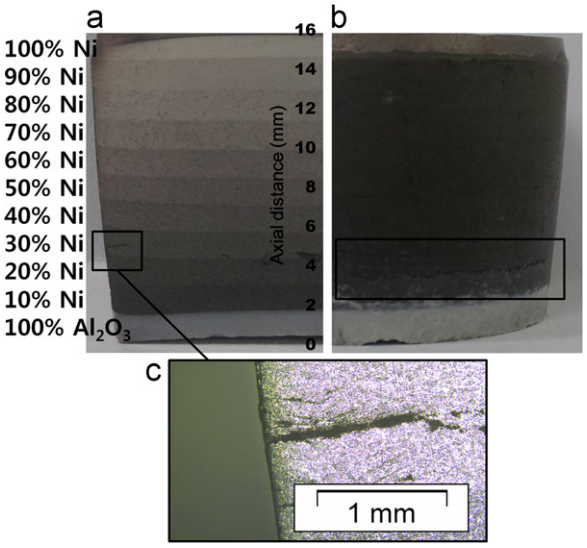

Fig. 6. Optical images of an FGM with a uniform volume proportional gradient (Sample A): (a) cross-sectional image, (b) external surface, and (c) magnified view of cracks.

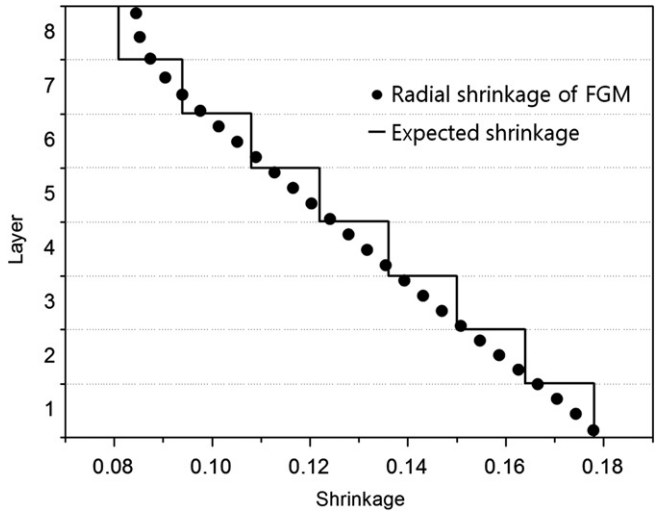

Fig. 7. Comparison of measured with expected radial shrinkages. The layer numbers along the *y*-axis correspond to the layers specified in Table 2.

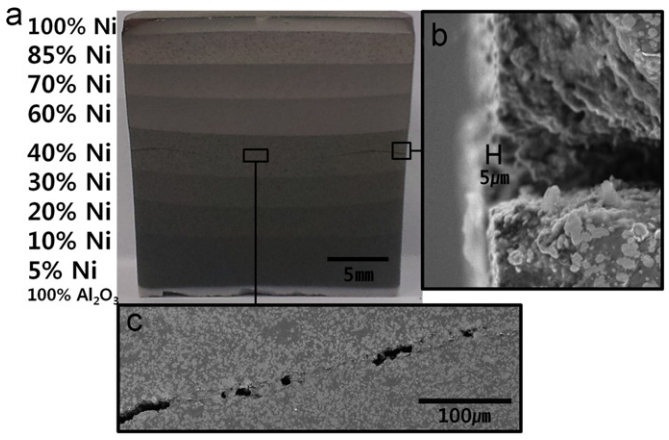

Fig. 8. FGM fabricated without a uniform shrinkage gradient (Sample B): (a) cross-sectional image, (b) magnified image, and (c) magnified image of the crack and pores.

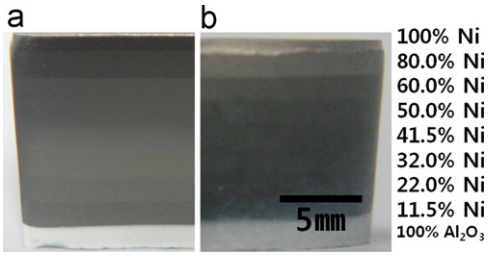

Fig. 9. FGM with a uniform shrinkage gradient (Sample C): (a) optical cross-sectional image and (b) Optical image of the surface.

Differences between the measured and expected radial shrinkages of the FGM are shown in Fig. 7. Figs. 7 and 9 show that the actual layer shrinkages were similar to their predicted values. Distortions caused by differential shrinkage were similar throughout those layers, except for the 100% Ni layer. This layer behaved differently for the

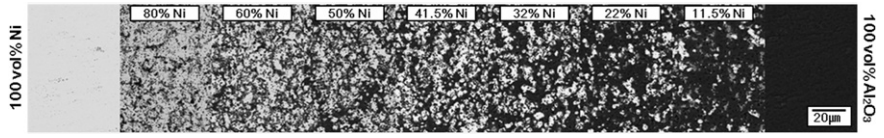

Fig. 10. Scanning electron microscopy (SEM) images in backscattering mode of an FGM (Sample C).

following reasons: first, 100% Ni begins to sinter at a much lower temperature than the other layers (Fig. 2). Sintering is complete at 1000 °C, while the other layers are just beginning to sinter at this temperature. Therefore, a significant amount of shrinkage was observed at 1000 °C for the 100% Ni layer. Second, the sintering stress for submicron Al_2O_3 [13,14] is generally much higher than that for micro-scale metals [11,15,16], and this has a dramatic effect on shrinkage during sintering. Hence, the influence of the 100% Ni layer on the other layers can be considered negligible, and thus 100% Ni was excluded from shrinkage considerations in Fig. 7.

The composition of the FGM (Sample B) shown in Fig. 8 was in accordance with a study by Park et al. [12]. The composition was designed to withstand the stress due to coefficient of thermal expansion (CTE) mismatch between adjacent layers. However, as shown in Fig. 8, a crack appeared in the middle of the sample due to different amounts of shrinkage within adjacent layers, possibly occurring during sintering rather than during the cooling process. Cracks are generated at points of severe shrinkage. Fig. 8(b) shows that there was a differential shrinkage mismatch of 5 μm. A crack was also observed for the composition of 30 vol% Ni/70 vol% Al_2O_3 (Fig. 6). Therefore, Samples A and B show that sequential grading of layers and designing layers to minimize thermal mismatch are not enough to eliminate the risk of crack development in a multi-layered FGM.

Finally, Sample C was designed to have a uniform shrinkage during sintering. Its optical image is shown in Fig. 9. This sample did not crack, indicating that the amount of distortion was uniform and controlled. SEM imaging in the backscattering mode of an FGM was used to confirm that the matrix (Al_2O_3) was distributed uniformly throughout the FGM (Fig. 10) and led to consistent shrinkage differences. Thus, the empirical formulation based on shrinkage was successfully used to fabricate a crack-free FGM.

4. Conclusions

The dimensional shrinkage in metal–ceramic FGMs was controlled to minimize distortion during sintering. Shrinkage was predicted based on the change in porosity in the sample during sintering. A relationship was established between dimensional shrinkage and material composition. By tailoring the material composition to provide a uniform shrinkage gradient across the entire sample, the number of internal cracks was dramatically reduced. Therefore, this uniform geometry model is useful for investigating sintering stress and distortion in multi-layer systems.

Acknowledgments

This work was supported by the Mid-Career Researcher Program through an NRF grant funded by the MEST (no. 2011–0000201) and by the Energy & Resource Recycling program grant (no. 20105020100010) of the Korean Institute of Energy Technology Evaluation and Planning funded by the Korean Ministry of Knowledge Economy and Basic Science Research Program through the National Research Foundation of Korea(NRF) funded by the Ministry of Education, Science and Technology (no. 2012032560).

References

[1] S. Suresh, A. Mortensen, Fundamentals of Functionally Graded Materials: Processing and Thermomechanical Behaviour of Graded Metals and Metal–Ceramic Composites, University Press, Cambridge, 1998.
[2] Y. Miyamoto, W.A. Kaysser, B.H. Babin, A. Kawasaki, R.G. Ford, Functionally Graded Materials: Design, Processing and Applications, Kluwer Academic Publishers, Boston, 1999.
[3] J.H. Song, S.D. Mun, Fracture characteristics of flame thermal shock in PSZ/NiCrAlY FGM, Korean Journal of Metals and Materials 48 (8) (2010) 775–779.
[4] Y.M. Shabana, M.L. Pines, H.A. Bruck, Modeling the evolution of stress due to differential shrinkage in powder-processed functionally graded metal–ceramic composites during pressureless sintering, International Journal of Solids and Structures 43 (2006) 7852–7868.
[5] R. Watanabe, Powder processing of functionally gradient materials, MRS Bulletin 20-1 (1995) 32–34.
[6] J.G. Kruft, Y.M. Shabanaand, H.A. Bruck, Effect of TiO_2 nanopowder on the sintering behavior of nickel–alumina composites for functionally graded materials, Journal of the American Ceramic Society 91 (9) (2008) 2870–2877.
[7] A.N. Winter, B.A. Corff, I.E. Reimanis, B.H. Rabin, Fabrication of graded nickel–alumina composites with a thermal-behavior-matching process, Journal of the American Ceramic Society 83 (9) (2000) 2147–2154.
[8] Z. He, J. Ma, G.E.B. Tan, Fabrication and characteristics of alumina–iron functionally graded materials, Journal of Alloys and Compounds 486 (2009) 815–818.
[9] D. Ravi, D.J. Green, Sintering stresses and distortion produced by density differences in bi-layer structures, Journal of the European Ceramic Society 26 (2006) 17–25.
[10] S.E. Schoenberg, D.J. Green, A.E. Segall, G.L. Messing, A.S. Grader, P.M. Halleck, Stress and distortion due to green density gradients during densification, Journal of the American Ceramic Society 89 (10) (2006) 3027–3033.
[11] R.M. German, Sintering Theory and Practice, John Wiley and Sons, New York, 1996.

[12] J.H. Park, J.C. Lee, S.H. Ryu, K.B. Jung, H.-B. Song, J.C. Yun, Y.H. Choa, S.H. Ahn, C.S. Lee, Crack-free joint in a Ni–Al_2O_3 FGM system using three-dimensional modeling, Materials Transactions 50 (7) (2009) 1875–1880.
[13] T. Ikegami, N. Iyi, I. Sakaguchi, Evaluation of sintering stresses of an Al_2O_3 powder with a self-loading apparatus, Ceramics International 35 (2009) 3185–3194.
[14] T. Ikegami, N. Iyi, I. Sakaguchi, Influence of magnesia on sintering stress of alumina, Ceramics International 36 (2010) 1143–1146.
[15] E.H. Aigeltinger, Relating microstructure and sintering force, International Journal of Powder Metallurgy and Powder Technology 11 (1975) 195–203.
[16] R.A. Gregg, F.N. Rhines, Surface tension and the sintering force in copper, Metallurgical Transactions 4 (1973) 1365–1374.
[17] M.L. Pines, H.A. Bruck, Pressureless sintering of particle-reinforced metal–ceramic composites for functionally graded materials: part I. Porosity reduction models, Acta Materialia 54 (2006) 1467–1474.